Materials Research Bulletin 46 (2011) 1346–1351

Contents lists available at ScienceDirect

Materials Research Bulletin

journal homepage: www.elsevier.com/locate/matresbu

# Synthesis and properties of $A_6B_2(OH)_{16}Cl_2{\cdot}4H_2O$ (A = Mg, Ni, Zn, Co, Mn and B = Al, Fe) materials for environmental applications

Anderson Dias *, Lumena Cunha, Andiara C. Vieira

*Departamento de Química, Universidade Federal de Ouro Preto, Campus Morro do Cruzeiro, ICEB II, Sala 67, Ouro Preto-MG, 35400-000, Brazil*

ARTICLE INFO

*Article history:*
Received 11 May 2010
Received in revised form 7 March 2011
Accepted 13 May 2011
Available online 23 May 2011

*Keywords:*
A. Oxides
B. Chemical synthesis
C. Raman spectroscopy

ABSTRACT

Double layered hydroxide materials of composition $A_6B_2(OH)_{16}Cl_2{\cdot}4H_2O$ (A = Mg, Ni, Zn, Co, Mn and B = Al, Fe) were synthesized by chemical precipitation at 60 °C. Different levels of crystallinity and ordering degree were observed depending upon the chemical environment or the combination between divalent and trivalent cations. The results from high-resolution transmission electron microscopy revealed that nanostructured layered samples were obtained with interplanar spacing compatible with previous literature. Raman scattering was employed to investigate the complex band structure observed, particularly the lattice vibrations at lower frequencies, which is intimately correlated to the cationic radius of both divalent and trivalent ions. The results showed that strongly coordinated water and chloride ions besides highly structured hydroxide layers have a direct influence on the stability of the hydrotalcites. It was observed that transition and decomposition temperatures varied largely for different chemical compositions.



## 1. Introduction

Anionic clays or layered double hydroxides (LDH) of general formula $[M^{+2}{}_{1-x}M^{+3}{}_x(OH)_2][A^{-m}]_{x/m}{\cdot}nH_2O$ constitute a class of hydroxyl-hydrated compounds formed by chemical substitution of divalent ions of the brucite-like octahedral layers by trivalent ions [1]. In these structures, the cations are located in the center of octahedra formed by six hydroxyl groups, while the anions and the water molecules are arranged into interlayer alternating with the octahedral sheets [1]. Recently, these materials have attracted much attention because of the tremendous potential for application in many areas of chemistry, particularly the environmental chemistry [2,3]. From the chemical point of view, the main function of these materials is their ability to accommodate different combinations of cations, which means different environments in the brucite-like layers and, thus, different chemical affinities into interlayer [4]. Particularly, these unlimited chemical changes allow a large variety of anionic species together with water molecules to enter inside the layers and, consequently, singular scientific and technological applications can be achieved [5–7]. In this respect, many papers show the morphological aspects and their relationship with industrial applications, like adsorbents and catalysts [8–11].

The most common layered materials investigated by the literature are a combination of divalent cations with aluminum and carbonate as guest anion [12]. Other works deal not only with mineral samples studying Fe, Cr and Mn as trivalent cation, but also with carbonates as guest anion [13–15]. LDH containing sulfate and, particularly, chloride ions as interlayer anions are less common, except for the Ca-hydrocalumite type materials, which are largely used in cement chemistry with sulfate anions inside the interlayer [16–18]. In a previous work [19], a sequence of layered materials were chemically synthesized with different divalent cations in the formula $A_6Al_2(OH)_{16}Cl_2{\cdot}4H_2O$ (A = Mg, Ni, Zn, Co, and Mn) and $Ca_2Al(OH)_6Cl{\cdot}2H_2O$. The aim was to study the structural properties of this series of compounds containing chloride ions into interlayer. Now, we focus our attention to the synthesis and spectroscopic properties of the $A_6Fe_2(OH)_{16}Cl_2{\cdot}4H_2O$ analogues. For the structural and vibrational analyses of the obtained materials, X-ray diffraction, thermal analysis, scanning and transmission electron microscopies, and Raman scattering were employed.

## 2. Experimental

LDH of nominal composition $A_6B_2(OH)_{16}Cl_2{\cdot}4H_2O$ (A = Mg, Ni, Zn, Co, Mn and B = Al, Fe) were synthesized by chemical coprecipitation. Stoichiometric amounts of high-purity $MeCl_2$, $FeCl_3$, $AlCl_3$ and NaOH (Aldrich Chemicals, Inc.) were separately dissolved in distilled water and mixed by vigorous stirring. The metal concentration in the solution was maintained at 2 mol/L

* Corresponding author. Tel.: +55 31 3559 1716; fax: +55 31 35591707.
*E-mail address:* anderson_dias@iceb.ufop.br (A. Dias).

0025-5408/$ – see front matter © 2011 Elsevier Ltd. All rights reserved.
doi:10.1016/j.materresbull.2011.05.022

during precipitation (pH = 10) by dropping, when necessary, a diluted solution of NaOH. The synthesis occurred by mixing the reactants previously dissolved in a glass reactor maintained at 60 °C, for 3 h. Following, the solution was filtered and washed with distilled water and finally dried at 70 °C under low-humidity environment (<30%) to guarantee the quality assurance. The resulting liquid and the precipitated solids were both chemically analyzed by inductively coupled plasma (ICP-OES) in Spectra CIROS CCD equipment. The solid samples were stored in sealed desiccators to prevent any water or $CO_2$ adsorption and preserve the quality of the samples. Elemental chemical analysis indicated that the molar ratios of divalent cation and Fe or Al in the precipitated samples were in perfect agreement with the theoretical value (divalent metal/trivalent metal = 3). Special care was taken to verify the experimental values of divalent metal and Al or Fe concentrations, since stoichiometric deviations could lead to erroneous interpretation of all subsequent results.

The crystal structure and phase purity of the as-synthesized samples were studied by X-ray diffraction (XRD) using a Shimadzu D-6000 diffractometer with graphite monochromator and a nickel filter in the range 5–70° 2$\theta$ (step 0.02° 2$\theta$), operating with Fe$K\alpha$ radiation ($\lambda$ = 0.19360 nm), 40 kV, 20 mA (the results were automatically converted to Cu$K\alpha$ radiation for data treatment and manipulation). Scanning and transmission electron microscopies were carried out to investigate the morphology of the samples. A Quanta 200 (FEI) field-emission scanning electron microscope (FE-SEM) was employed to analyze the morphology of layered materials (30 kV), while a Tecnai G2-20 (FEI) transmission microscope (TEM) was used to study the morphologies and crystalline aspects of the samples (200 kV). The materials were dispersed in an alcoholic solution and submitted to ultrasound prior to be placed in holey carbon–copper grids (300 mesh). High-resolution TEM (HRTEM) was obtained in the same Tecnai G2-20 equipment at accelerating voltages of 200 kV.

Simultaneously thermal analyses were carried out with a DTA/TG (TA Instruments SDT 2960), from room temperature to 1100 °C, under nitrogen atmosphere and heating rates of 20 °C/min. Around 7 mg of each sample were weighed and placed in an alumina crucible. Raman spectra were collected in back-scattering configuration by using a Horiba/Jobin-Yvon LABRAM-HR spectrometer, equipped with a 632.8 nm line of a helium–neon laser (power of 18 mW) as an excitation source, 600 and 1800 grooves/mm diffraction gratings, Peltier-cooled CCD detector and a confocal Olympus microscope (100× objective). An edge filter was used to stray light rejection (Rayleigh scattered light). Repeated analyses were done beginning with very low laser powers to prevent damage in the samples; the laser power was incrementally increased after each set of analyses. In this way, untouched surfaces were studied for determination of the better signal/noise ratio without creation of new phases through laser heating of the samples in the presence of oxygen (air). The best conditions for analyses, including a slight defocusing of the laser, were found at 0.18 mW of laser power through 10 accumulations of 30 s each. The obtained spectra were corrected by the Bose–Einstein thermal factor [20].

## 3. Results and discussion

Fig. 1 presents the XRD patterns of the hydrotalcites obtained by chemical coprecipitation. The results showed that all syntheses were successful and single-phase materials with general formula $A_6B_2(OH)_{16}Cl_2{\cdot}4H_2O$ (A = Mg, Ni, Zn, Co, Mn and B = Al, Fe) were produced. The samples were indexed by the only available ICDD cards 19-0748 (MgAl), 20-0500 (MgFe), 55-0039 (NiAl), 49-0721 (NiFe), and 57-0045 (ZnAl). There are no existing ICDD cards for Co and Mn compounds. Sharp and relatively symmetric reflections for

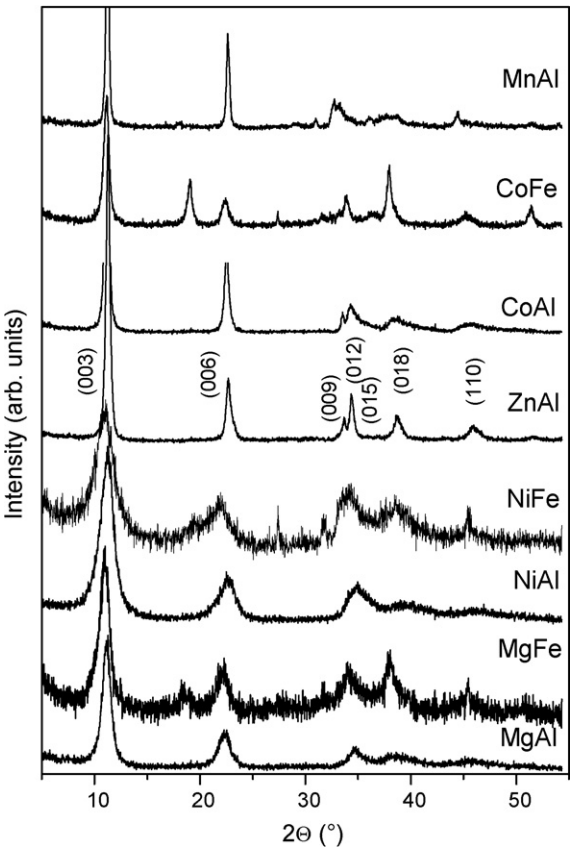


**Fig. 1.** XRD data for the hydrotalcites obtained by chemical synthesis at 60 °C. The main crystallographic planes are indicated for the Zn hydrotalcite [$Zn_6Al_2(OH)_{16}Cl_2{\cdot}4H_2O$].

the basal planes (0 0 3) and (0 0 6), beside broad and asymmetric reflections for the non-basal (0 1 2), (0 1 5), and (0 1 8) planes are seen. The presence of broad basal planes indicates that the materials are crystalline and also formed by small crystallites. On the other hand, the presence of non-basal planes of the family (0 $k$ $l$) could suggest the occurrence of stacking faults in the structure of the LDH [21]. In this work, MgAl, MgFe, NiAl and NiFe materials exhibited the broadest basal peaks among the samples produced, indicating smaller crystallites. Asymmetric peaks in the region around 34° 2$\theta$ caused an overlap of the planes (0 0 9)/(0 1 2) and could indicate the presence of stacking faults, as discussed in our previous publications [19,23]. For ZnAl materials (see Fig. 1), it is possible to discern both peaks, while for all other samples the asymmetry is observed. According to Hines et al. [22], the analysis of the (0 0 6) basal planes would indicate the presence of carbonates together with chloride ions in the hydrotalcites. Multiple peaks associated with this basal plane represent distinct basal spacings, which correspond to chloride-rich and carbonate-rich regions within a given sample [22].

Cell parameters were calculated by using XRD data and correlated to the chemical composition: the $a$-parameter represents the average cation–cation distance within the brucite-like layers and can be obtained by $a = 2d_{1\,1\,0}$; the $c$-parameter is related to the thickness of the brucite-layer and the interlayer distance, and can be better determined by the formula $c = 3/2(d_{0\,0\,3} + 2d_{0\,0\,6})$ [19]. The observed interplanar spacings used for the determination of the cell parameters were corrected using Si as an external standard, ICDD card 27-1402. The results are displayed in Table 1, showing that different chemical compositions produced hydrotalcites with different cell parameters, depending

**Table 1**
Cell parameters calculated from XRD, transition temperatures and weight losses (observed and calculated) determined by thermal analyses as function of chemical composition and cationic radii for all hydrotalcites.

| LDH | Cell parameters (Å) | | $T_1$ (°C) | Observed $WL_1$ (%) | Calculated $WL_1$ (%) | $T_2$ (°C) | $WL_2$ (%) |
|---|---|---|---|---|---|---|---|
| | *a* | *c* | | | | | |
| MgAl | 3.11 | 23.90 | 110/110 | 16.0 | 11.7 | 410/401 | 14.0 |
| MgFe | 3.11 | 24.08 | 86/67 | 12.7 | 12.0 | 330/325 | 18.0 |
| NiAl | 3.05 | 23.56 | 106/111 | 13.0 | 8.8 | 331/319 | 17.0 |
| NiFe | 3.08 | 24.09 | 89/71 | 11.3 | 8.9 | 265/258 | 14.8 |
| ZnAl | 3.08 | 23.50 | 127/130 | 8.0 | 8.4 | 265/257 | 15.0 |
| CoAl | 3.09 | 23.66 | 106/112 | 8.9 | 8.8 | 219/212 | 7.0 |
| CoFe | 3.12 | 23.66 | 88/68 | 9.5 | 8.9 | 254/239 | 12.2 |
| MnAl | 3.11 | 23.59 | 94/101 | 8.0 | 9.0 | 219/234 | 13.0 |

$T_1$ = first transition temperature from DTA signal/TG derivative. $T_2$ = second transition temperature from DTA signal/TG derivative. $WL_1$ and $WL_2$ = weight losses related to first and second transition.

on the ionic radii (compiled from Bellotto et al. [21] and Shannon [24]), as expected. It is important to note that the ionic radii of Ni, Co and Zn are very close for a six-fold coordination (octahedral sites) [21,24], which sometimes difficult for the interpretation of the XRD data. Nevertheless, the calculated cell parameters of all samples are in agreement with those reported in the literature [6,7,16,21].

Fig. 2 presents a FE-SEM image for the MgFe hydrotalcite, where it can be seen a very fine, plate-like (layered) morphology. All samples exhibited the same morphological features, thus indicating that the layered structure can be obtained independently of the cation combination. Fig. 3 presents FE-SEM and TEM images for the homologous MgAl hydrotalcite. Fig. 3a shows a nanometer-sized particle, which is also formed by very fine flakes. A particular area of this sample (represented by the open square in Fig. 3a) was investigated in detail by HRTEM and the results are displayed in Fig. 3b. As it can be noted, the presence of two-dimensional lattice fringes clearly illustrate that the materials obtained are polycrystalline (diffuse, concentric rings showed in Fig. 3b) with computed interplanar spacings of about 8.0 Å, which corresponds to the (0 0 3) basal planes. Fig. 4 presents a set of images obtained by FE-SEM and HRTEM for Fe-based hydrotalcites. MgFe materials presented a plate-like (layered) morphology (Fig. 4a) with interplanar spacings of about 8.1 Å (Fig. 4b), which is in agreement with XRD data (Table 1). For the samples with Ni (Fig. 4c) and Co (Fig. 4d), interplanar spacings of the same order of magnitude were computed, in agreement with the literature and our experimental XRD data.

Thermal analyses revealed endothermic peaks (DTA signal) together with weight losses in the thermogravimetric profiles (TG),

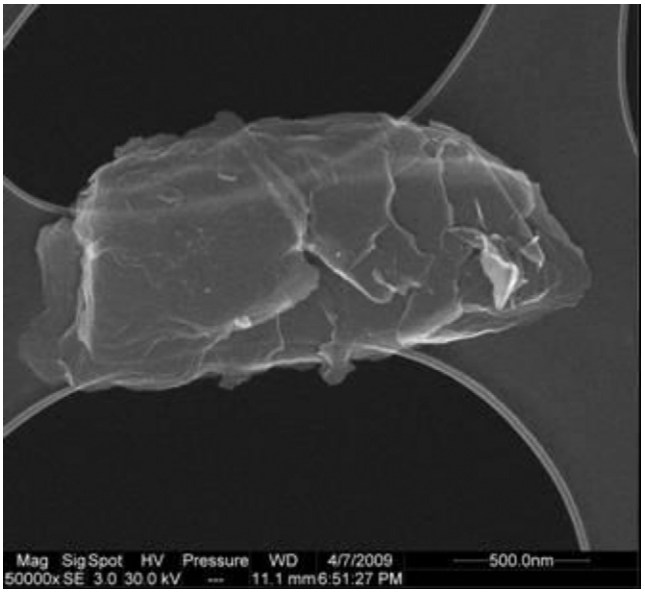


**Fig. 2.** FE-SEM image for the MgFe hydrotalcite synthesized at 60 °C.

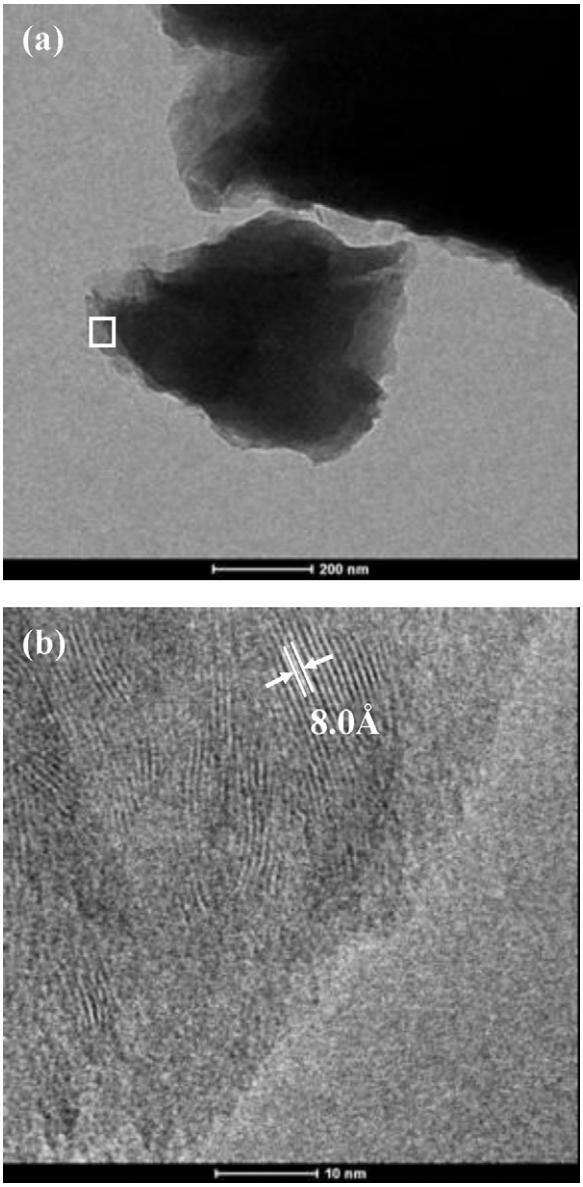


**Fig. 3.** (a) FE-SEM and (b) TEM images for the MgAl layered material. The open square in (a) represents the area investigated by HRTEM and displayed in (b).

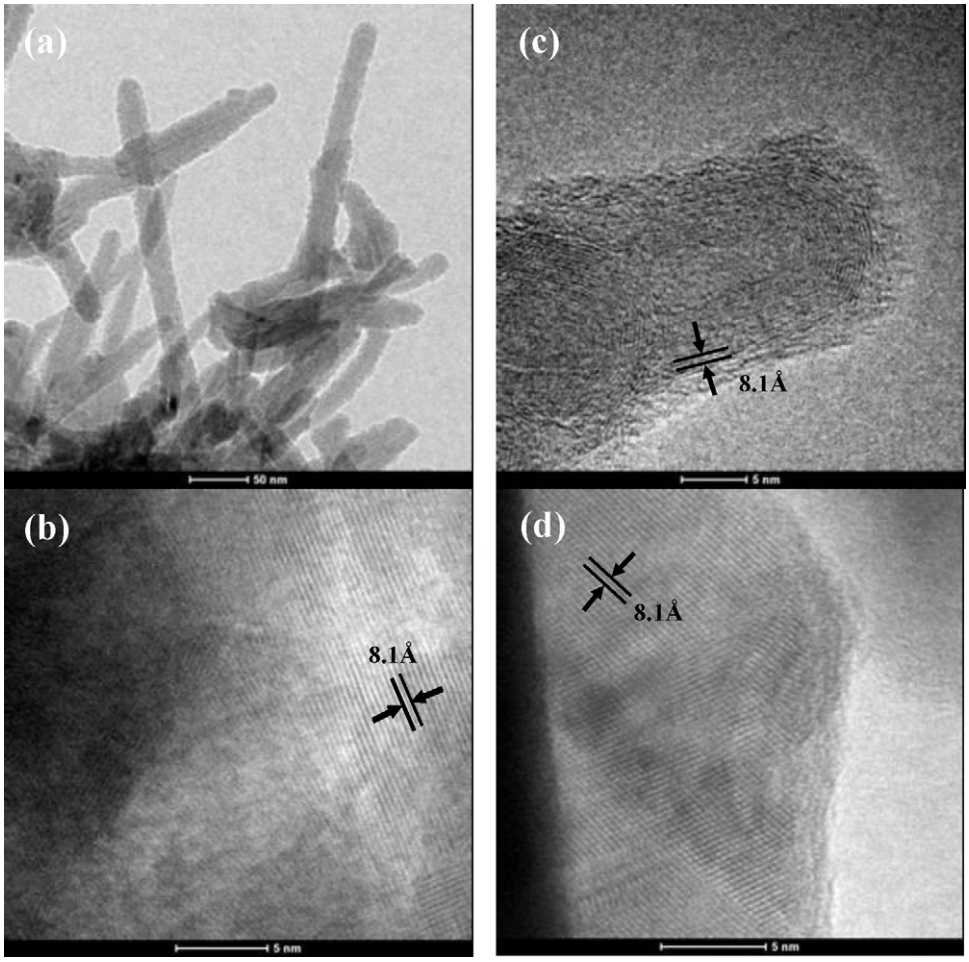


**Fig. 4.** (a) and (b) show FE-SEM and HRTEM images, respectively, for the MgFe sample. HRTEM images for the samples NiFe and CoFe are displayed in (c) and (d), respectively.

as expected. These hydration–dehydration dynamics are typical in hydrotalcites, which contain water molecules and hydroxyl groups in their structure [7,25–27]. Kirkpatrick et al. [25–27] studied the hydration energies of these systems as a function of different intercalated species, showing that they are directly related to the electrostatic interactions and the H-bonding into the structure. For our samples, the dehydration behavior was studied aiming to correlate with the structural features analyzed through optical spectroscopic techniques. The peaks in DTA profiles (transition temperatures) are in perfect agreement with the derivative of the weight loss (TG) for all samples. If the quantification of the water molecules for each hydrotalcite could be determined, the results would help us to interpret the XRD and spectroscopic data. Fig. 5 presents the TG curves and their respective DTA signal for all materials. The values for the two main transition temperatures and weight losses are indicated in Table 1, beside the quantification of the water molecules into interlayers. The two main sharp transitions are of special interest, since they are related to the release of the water molecules present in the interlayer (for some samples, these releases occur as several steps) and to the process of dehydroxylation of the hydroxide layers [23,28].

The release of water molecules permits one to determine the number of units present in the interlayers. As can be seen in Fig. 5 and Table 1, the first weight loss occurred at around 100 °C (between 86 and 127 °C, for MgFe and MnAl hydrotalcites), while the second one occurred in the range 219–410 °C (MnAl-CoAl and MgAl) and corresponds to the dehydroxylation of the brucite-like sheets. For MgAl and NiAl materials, the weight losses were higher than expected from the nominal compositions (four water molecules). As verified in our previous work by infrared spectroscopy (FTIR) in similar samples [19], these additional losses are due to the decarbonation process (here assumed as an impurity). Now, a brief discussion concerning the distance between the observed temperature transitions in our hydrotalcites must be given. Depending on the atmosphere employed, these transitions can move and become closer if, for example, air is used as a decomposition atmosphere [28]. In this work, the heating process was conducted under a nitrogen atmosphere. Samples with MgAl and NiFe presented the largest differences between 1st and 2nd transitions (300 °C and 276 °C, respectively). No losses could be observed between the main transitions, which could be an indication of very stable structures. The hydrotalcite with ZnAl and MnAl present similar differences of about 130 °C. MnAl and CoAl materials present the closest transition temperatures (113–125 °C). A similar behavior was previously verified in Co hydrotalcites with carbonates [28], and was attributed to the presence of $Co^{+2}$ in the brucite-like sheets, which can be easily oxidized. It is believed that the same type of oxidation could occur with Mn ions, thus destabilizing the hydrotalcite structures of these compounds.

Fig. 6 presents the Raman spectra of Fe-based hydrotalcites in the wavenumber region 150–1050 $cm^{-1}$. For these materials, a detailed discussion was published recently [19], in which a complex band structure with significant differences between the samples was observed. According to Lin et al. [29] and Richardson and Braterman [30], the hydroxide layers can be assumed to be composed of many tripod units of $A_3OH$, such as $A_3OH$ (A = divalent cation), $Fe_3OH$, $Fe_2AOH$, $A_2FeOH$ (called $A_3$-coordinated and

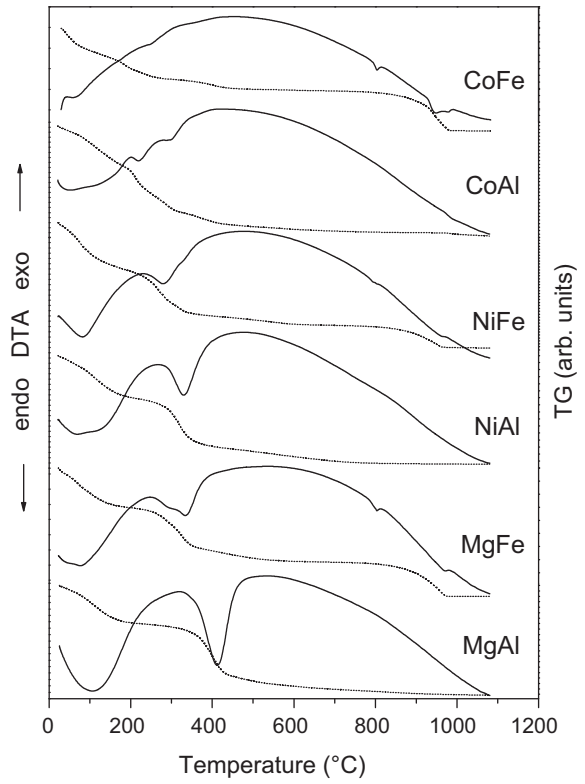


**Fig. 5.** Thermal analysis of the hydrotalcites as a function of composition. DTA signal (solid curves) and weight losses (dotted curves) are indicated in arbitrary units only for qualitative comparison. Transition temperatures are given in Table 1.

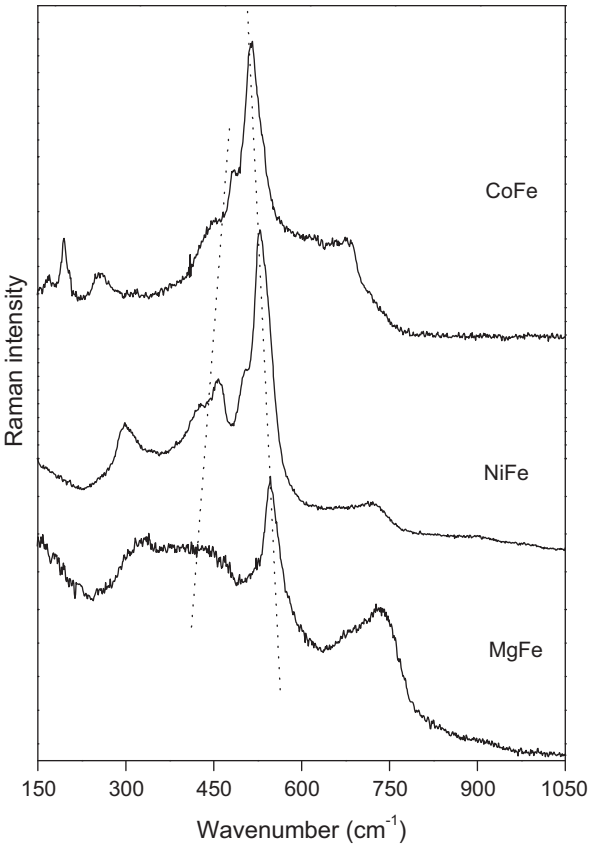


**Fig. 6.** Raman spectra for the Fe-based samples in the wavenumber region 150–1050 $cm^{-1}$. The dotted lines are guide for the eyes, showing the opposite behavior for the two main bands.

$A_2Fe$-coordinated units). For the wavenumber region showed in Fig. 6, the most relevant bands are located at around 470 $cm^{-1}$ ($A_{1g}$) and 560 $cm^{-1}$ ($E_g$), which correspond to symmetric vibrations of Fe-OH bonds [28]. Carbonate-related bands, in particular the band at 1060 $cm^{-1}$ and the antisymmetric stretching vibration around 1390 $cm^{-1}$, were not observed in our samples. This result confirms the low-contamination level with carbonates. Sampieri et al. [31] reported the carbonate-phobic character of ZnAl and MnAl nitrated hydrotalcites, showing that this behavior is because of the poor basicity (electronegativity) of the brucite-like layers. We believe that the same behavior could be expected for all other materials, i.e., the different basicity could produce different carbonate-phobic characters depending upon the chemical composition. In this sense, Mg-containing compounds could be less phobic (more electronegative) and, thus, could exhibit a higher tendency to carbonate contamination. A final remark for the Raman modes between 400 and 650 $cm^{-1}$, which are related to Fe-OH vibrations, must be given. For these bands, a slight decreasing tendency was observed in frequency of increasing ionic radius for the band around 550 $cm^{-1}$, while the opposite behavior was verified for the mode around 470 $cm^{-1}$. This result confirms the supposition by many authors in the hydrotalcite literature that these bands possibly could be influenced by the divalent cations [28]. Similar results were previously observed by Pérez-Ramírez et al. [28] for Ni and Co hydrotalcites with nitrate ions in the interlayer. However, the authors did not comment on this behavior, probably because only two chemically substituted samples were studied.

## 4. Conclusions

LDH materials of general formula $A_6B_2(OH)_{16}Cl_2{\cdot}4H_2O$ (A = Mg, Ni, Zn, Co, Mn, and B = Al, Fe) were synthesized at 60 °C. Crystalline, single-phase materials were obtained and studied by techniques such as XRD, FE-SEM, HRTEM, thermal analysis, and Raman spectroscopy. A description of the structure of all samples produced was accomplished by correlating the results of all techniques employed. XRD and thermal analyses showed that the hydrotalcites produced are different as regards to their crystallinity and order. ZnAl hydrotalcite was interpreted as the most crystalline among the produced materials without stacking faults, while MgFe and NiFe materials presented broader, and asymmetric XRD peaks, which were attributed to their lower ordering, smaller crystallite size and high level of stacking faults. Raman spectroscopy showed a complex band structure, which can be related to the cationic radius. The results showed that strongly coordinated water and chloride ions besides highly structured hydroxide layers have a direct influence on the stability of the hydrotalcites. It was observed that transition and decomposition temperatures varied largely for different chemical compositions.

## Acknowledgements

The authors acknowledge the financial support from CNPq, FINEP and FAPEMIG. Special thanks to the Center of Microscopy – UFMG for technical support with electron microscopy.

## References

[1] G. Renaudin, M. François, Acta Crystallogr. C: Cryst. Struct. Commun. 55 (1999) 835.
[2] H.C. Greenwell, W. Jones, P.V. Coveney, S. Stackhouse, J. Mater. Chem. 16 (2006) 708.
[3] M. Balakrishnan, V.S. Batra, J.S.J. Hargreaves, I.D. Pulford, Green Chem. 13 (2011) 16.
[4] M. Wei, M. Pu, J. Guo, J.B. Han, F. Li, J. He, D.G. Evans, X. Duan, Chem. Mater. 20 (2008) 5169.
[5] K.H. Goh, T.T. Lim, Z. Dong, Water Res. 42 (2008) 1343.

[6] X.X. Guo, F.Z. Zhang, D.G. Evans, X. Duan, Chem. Commun. 46 (2010) 5197.
[7] S.J. Palmer, R.L. Frost, T. Nguyen, Coord. Chem. Rev. 253 (2009) 250.
[8] J.A. Ritter, A.D. Ebner, Sep. Sci. Technol. 42 (2007) 1123.
[9] P. Nalawade, B. Aware, V.J. Kadam, R.S. Hirlekar, J. Sci. Ind. Res. 68 (2009) 267.
[10] M.L. Occelli, J.P. Olivier, A. Auroux, M. Kalwei, H. Eckert, Chem. Mater. 15 (2003) 4231.
[11] P.J. Sideris, U.G. Nielsen, Z.H. Gan, C.P. Grey, Science 321 (2008) 113.
[12] U. Sharma, B. Tyagi, R.V. Jasra, Ind. Eng. Chem. Res. 47 (2008) 9588.
[13] J.W. Boclair, P.S. Braterman, Chem. Mater. 11 (1999) 298.
[14] E. Géraud, S. Rafqah, M. Sarakha, C. Forano, V. Prevot, F. Leroux, Chem. Mater. 20 (2008) 1116.
[15] L. Obalova, K. Jiratova, F. Kovanda, K. Pacultova, Z. Lacny, Z. Mikulova, Appl. Catal. B: Environ. 60 (2005) 289.
[16] G.M. Lombardo, G.C. Pappalardo, Chem. Mater. 20 (2008) 5585.
[17] T. Kameda, T. Yoshioka, K. Watanabe, M. Uchida, A. Okuwaki, Appl. Clay Sci. 37 (2007) 215.
[18] R. Mostarih, A. de Roy, J. Phys. Chem. Solids 67 (2006) 1058.
[19] A.C. Vieira, R.L. Moreira, A. Dias, J. Phys. Chem. C 113 (2009) 13358.
[20] W. Hayes, R. Loudon, Scattering of Light by Crystals, Wiley, New York, 1978.
[21] M. Bellotto, B. Rebours, O. Clause, J. Lynch, D. Bazin, E. Elkaim, J. Phys. Chem. 100 (1996) 8527.
[22] D.R. Hines, S.A. Solin, U. Costantino, M. Nocchetti, Phys. Rev. B 61 (2000) 11348.
[23] A. Dias, R.G. Sá, M.C. Spitale, M. Athayde, V.S.T. Ciminelli, Mater. Res. Bull. 43 (2008) 1528.
[24] R.D. Shannon, Acta Crystallogr. A: Found. Crystallogr. 32 (1976) 751.
[25] P.P. Kumar, A.G. Kalinichev, R.J. Kirkpatrick, J. Phys. Chem. B 110 (2006) 3841.
[26] J.W. Wang, A.G. Kalinichev, R.J. Kirkpatrick, Geochim. Cosmochim. Acta 70 (2006) 562.
[27] P.P. Kumar, A.G. Kalinichev, R.J. Kirpatrick, J. Phys. Chem. C 111 (2007) 13517.
[28] J. Pérez-Ramírez, G. Mul, J.A. Moulijn, Vib. Spectrosc. 27 (2001) 75.
[29] Y.H. Lin, M.O. Adebajo, J.T. Kloprogge, W.N. Martens, R.L. Frost, Mater. Chem. Phys. 100 (2006) 174.
[30] M.C. Richardson, P.S. Braterman, J. Phys. Chem. C 111 (2007) 4209.
[31] A. Sampieri, G. Fetter, H. Pfeiffer, P. Bosch, Solid State Sci. 9 (2007) 394.